Role of Oncogenic Long Noncoding RNA KCNQ1OT1 in Colon Cancer

Gang Liu
The First Affiliated Hospital of Wannan Medical College
Lei Shi
The First Affiliated Hospital of Wannan Medical College
Bin Wang
The First Affiliated Hospital of Wannan Medical College
Zehui Wu
The First Affiliated Hospital of Wannan Medical College
Haiyuan Zhao
The First Affiliated Hospital of Wannan Medical College
Tianyu Zhao
Stomatological Hospital of Chongqing Medical University
Lianghui Shi (slh1020@163.com)
The First Affiliated Hospital of Wannan Medical College

Research Article

Keywords: lncRNA KCNQ1OT1, colon cancer, HCT116 cells, tumorigenesis

Posted Date: April 15th, 2022

DOI: https://doi.org/10.21203/rs.3.rs-1550314/v1

Abstract

lncRNA KCNQ1 opposite strand/antisense transcript 1 (KCNQ1OT1) plays critical roles in the tumorigenesis of various human cancers including colorectal. However, the role of KCNQ1OT1 in colon cancer requires further investigation. Retroviral vector pSEB61 was introduced to established HCT116-siKCN cells. Cellular proliferation was measured using crystal violet staining, and cell cycle was detected using flow cytometry (FCM). RNA sequencing (RNA-Seq) analysis revealed differentially expressed genes (DEGs). Gene ontology (GO) and Kyoto Encyclopedia of Genes and Genomes (KEGG) pathway enrichment analyses were performed to analyze enriched functions and singlaing pathways. RT-qPCR, immunofluorescence, and western blotting were used to validate downstream genes expression. Tumor xenografts in BALB/c nude mice were used to evaluate tumorigenesis effects. Our data revealed that silencing KCNQ1OT1 in HCT116 cells slowed cell growth and decreased the distribution of cells in the G2/M phase. RNA-Seq analysis results indicated the transcript data of DEGs enriched in various GO and KEGG pathways, including DNA replication and cell cycle. RT-qPCR, immunofluorescence, and western blotting results validated the downstream CCNE2, PCNA, and BCL2. HCT116-siKCN cells markedly suppressed tumorigenesis in BALB/c nude mice. Our study suggest that lncRNA KCNQ1OT1 may provide a promising therapeutic strategy for colon cancer.

Introduction

In humans, approximately 2% of RNA transcripts are protein-coding genes. Additionally, most RNA transcripts are defined as noncoding RNAs, which can be divided into short noncoding RNAs and long noncoding RNAs (lncRNAs) that are longer than 200 nucleotides in length and lack an open reading frame (ORF)[1–3]. Although lncRNAs are less abundant than mRNA, they can regulate protein-coding and noncoding gene expression and interact with RNA/DNA-binding proteins, transcription factors, and microRNA (miRNA)[4,5]. To date, only about 200 of an estimated 60,000 – 100,000 lncRNAs have been the focus of research, especially in cancer development and progression[6,7]. Accumulating evidence suggests that targeting oncogenic lncRNAs may provide a prospective application for the treatment of cancers[8–10]. Colon cancer remains a leading cause of death in China, and further research is required to elucidate the mechanisms underlying the development of this cancer and identify novel targets for advanced therapy.

lncRNA KCNQ1 opposite strand/antisense transcript 1 (KCNQ1OT1) is located on chromosome 11p15.5. KCNQ1OT1 mediates methotrexate resistance in HT29 and Caco2 colon cancer cell lines and promotes oncogenic properties in SW480 and DLD1 colon cancer cell lines[11,12]. With the development of bioinformatics, RNA sequencing (RNA-Seq) can be used to analyze global transcript data to investigate KCNQ1OT1-mediated oncogenicity in colon cancer cells.

Recent studies in which lncRNA KCNQ1OT1 in colon cancer cells was knocked down were mainly dependent on transient transfection with small interfering RNAs (siRNAs) using Lipofectamine. Therefore, the indefinite effects of KCNQ1OT1 silencing were dependent on the efficiency of transient transfection.

Retroviral systems provide a stable, credible, and long-term solution to assess the mechanisms through which KCNQ1OT1 plays a role in colon cancer oncogenicity both *in vitro* and *in vivo*.

In the current study, we established the HCT116-siKCN stable cell line with retroviral vector pSEB61 to explore the downstream genes of lncRNA KCNQ1OT1 and their contribution to the colon cancer phenotype. Our data revealed that KCNQ1OT1 silencing inhibited the growth of HCT116 cells and decreased the proportion of cells in the G2/M phase. RNA-Seq analysis, RT-qPCR, immunofluorescence, and western blotting were used to validate the downstream genes. Our data revealed that lncRNA KCNQ1OT1 plays a critical role in colon cancer development and targeting it could provide a potential option for clinical therapy.

Results

Establishing the HCT116-siKCN stable cell line

The three siRNA sequences are listed in Figure 1A. Three siRNAs targeting the lncRNA KCNQ1OT1 (NR_002728.3) were constructed using the pSEB61 vector, which contains the U6 and H1 promoters to drive siRNA expression (Figure 1B). The three plasmids containing siRNAs were packaged in a retrovirus. The concentration of blasticidin S for the positive selection of HCT116-siKCN cells was dependent on its minimum lethal dose in HCT116 cells. Finally, stable HCT116-siKCN cells were obtained by selection with blasticidin S (0.5 μg/ml) after culturing twice in McCoy's 5A medium containing 2% FBS for 3 days. RT-qPCR was used to verify silencing efficiency in HCT116-siKCN cells for further experiments (Figure 1D).

siRNA-KCNQ1OT1 inhibits cell proliferation and decreases the proportion of cells in the G2/M phase

Crystal violet staining was performed to determine the role of KCNQ1OT1 in HCT116 cell proliferation. We found that when seeded at a similar initial density, HCT116-siKCN cells reached confluence slower than HCT116 cells (Figure 2A). Quantitative assessment of the stained cells indicated that significantly fewer HCT116-siKCN cells appeared at 48, 72, and 96 h than HCT116 cells (Figure 2B). Collectively, these results showed that the proliferation of HCT116 cells was inhibited by siRNA-KCNQ1OT1 transfection. Next, the cell cycle was analyzed using flow cytometry. As shown in Figure 2C and 2D, the proportion of HCT116-siKCN cells in the G2/M phase was significantly decreased ($P < 0.001$). The proportion of cells in the G0/G1 and S phases between HCT116-siKCN and HCT116 cells did not differ significantly, suggesting that the downregulation of KCNQ1OT1 expression reduced the proportion of cells in the G2/M phase but not in the G0/G1 or S phase.

Analysis of DEGs between HCT116 and HCT116-siKCN cells

lncRNAs can regulate gene expression differentially through their interactions with DNA, miRNA, mRNA, and proteins. To further analyze the molecular mechanisms through which KCNQ1OT1 affects HCT116 cell proliferation and cycle distribution, RNA-Seq and bioinformatic analyses were performed. The expression of known genes was calculated using FPKM. After quality control, we obtained 12906 genes

in HCT116 cells and 13032 genes in HCT116-siKCN cells (FPKM ≥ 1). The FPKM of more than 60% of the genes was less than 1. The PCA diagram highlights the similarity degree between samples through dimensional reduction (Figure 3A). The heatmap indicates clusters from differences in mRNA expression between the two cell lines (Figure 3B). We identified 577 DEGs by fold-change filtering (|log2(fold change)|> 1), and Student's *t*-test ($P < 0.05$), Scatter plot (Figure 3C), and Volcano plot (Figure 3D) were used to visualize significant DEGs between HCT116 and HCT116-siKCN cells. Compared with HCT116-siKCN cells, 353 DEGs were significantly downregulated, while 224 DEGs were significantly upregulated in HCT116 cells.

To evaluate these differences, DEGs were analyzed at the functional level. Firstly, the enrichment of DEGs in different gene ontology (GO) functions were analyzed (Figure 4A). The top 20 GO terms suggested significant enrichment in DNA replication initiation, DNA−dependent DNA replication, sister chromatid segregation, nuclear chromosome segregation, DNA replication, chromosome segregation，nuclear division, organelle fission, mitotic cell cycle phase, cell cycle phase transition, mitotic cell cycle phase transition, cell cycle phase, biological phase, mitotic cell cycle process, mitotic cell cycle, chromosome, cell cycle process, chromosomal part, DNA metabolic process, and cell cycle.

Furthermore, KEGG pathway analysis results revealed that significant DEGs were mainly associated with cell cycle, DNA replication, fanconi anemia pathway, homologous recombination, ABC transporters, p53 signaling pathway, Nucleotide excision repair, IL−17 signaling pathway, Retinol metabolism, ECM−receptor interaction, Antigen processing and presentation, HTLV−I infection, Rheumatoid arthritis, Protein processing in endoplasmic reticulum, TNF signaling pathway, Apoptosis, Viral carcinogenesis, PI3K−Akt signaling pathway, Cytokine−cytokine receptor interaction (Figure 4B).

Disease enrichment demonstrated that lncRNA-KCNQ1OT1 showed significant associations with treatment of malignant neoplasm of breast, neoplasm metastasis, breast carcinoma, colon carcinoma, multiple myeloma, malignant neoplasm of ovary, liver carcinoma, ovarian carcinoma, malignant neoplasm of urinary bladder, and carcinogenesis (Figure 4C). In total, 102 DEGs were identified in colon carcinoma

Validation of downstream targets of DNA replication and cell cycle pathways

We obtained 19 DEGs enriched in DNA replication and the cell cycle pathway for RT-qPCR-based validation (Figure 5). Quantitative assessment confirmed that the expression of *PCNA*, *SKP2*, *ORC6*, *TTK*, *MCM3*, *MCM4*, *MCM7,* and *CCNE2* was decreased in HCT116-siKCN cells.

CCNE2 and PCNA are the two targets of KCNQ1OT1 regulators to promote cell proliferation in breast cancer and glioma. Immunofluorescence staining was used to detect protein localization in HCT116 and HCT116-siKCN cells. We found that PCNA and CCNE2 expression was high in the nucleus (Figure 6A). Positive cell counts did not differ significantly between HCT116 and HCT116-siKCN cells (data not shown). Western blotting was performed to further assess the quantity of protein expression in the two cell lines. As shown in Figure 6B, the expression of CCNE2 and PCNA appeared decreased.

Moreover, it was reported that the expression of the anti-apoptotic protein, BCL2, was reduced, while that of the apoptotic effector, CASP3, was elevated in SW480 and LS1034 cells. Western blotting results showed reduced BCL2 and cleaved CASP3 expression, but no significant difference was observed in pro-CASP3 expression in HCT116-siKCN cells (Figure 6B).

siRNA-KCNQ1OT1 ablates cellular vitality and tumor xenograft *in vivo*

Finally, we established a xenograft model to demonstrate the role of KCNQ1OT1 in cellular vitality and tumorigenesis *in vivo*. Ad-FLuc was introduced to establish HCT116-NC-FLuc and HCT116-siKCN-FLuc cells to observe the vitality of cells *in vivo*. Signals from bioluminescence images were readily detected in both groups at day 2 after injection, while these signals disappeared in HCT116-siKCN-FLuc-injected mice at day 14. Compared with HCT116-NC-FLuc-injected mice, the bioluminescence signals decreased significantly at day 14. Twenty days after injection, the mice were sacrificed, and the tumors were collected for further measurement. We also found that the volume of tumor xenografts in the HCT116-siKCN group was significantly decreased at day 14. Moreover, the tumor xenografts in the HCT116-siKCN group almost disappeared at day 30 after injection. Immunohistochemical staining of sections from tumor xenografts was also performed. The results revealed that the proportion of both PCNA- and CCNE2-positive cells were decreased in the HCT116-siKCN group.

Discussion

In the present study, we successfully established HCT116-siKCN cells with downregulated lncRNA KCNQ1OT1 expression compared with HCT116 cells. Accumulating evidence has indicated that the downregulation of KCNQ1OT1 expression in HCT116 cells may inhibit cell proliferation, reduce the proportion of cells in the G2/M phase *in vitro*, and significantly decrease tumor size and cellular vitality in ectopic xenografts in nude mice. To further explore the downstream genes, we summarized the global transcript data of the two cell lines to analyze and validate DEGs. Our results suggest that silencing KCNQ1OT1 in HCT116 cells may suppress tumor progression.

Colon cancer is one of the five most commonly diagnosed digestive cancers in China[13]. Noncoding RNAs can be divided into short noncoding RNAs and lncRNAs, which are more than 200 nucleotides in length. Owing to their abnormal expression, lncRNAs can function as tumor suppressors or oncogenic regulators in various cancers, including colon cancer[8, 14–16]. lncRNAs have the potential to serve as promising diagnostic or prognostic biomarkers and therapeutic targets for colon cancer. Approximately 200 differentially expressed lncRNAs involved in patient outcome and drug resistance in colon cancer have been obtained from The Cancer Genome Atlas[13,17]. However, the current understanding of the role of KCNQ1OT1 in colon cancer remains incomplete[18,19]. The present study aimed to perform a global bioinformatics analysis of downstream genes to explore the molecular mechanisms through which KCNQ1OT1 is involved in the tumorigenesis of colon cancer.

Previous studies have indicated that lncRNA KCNQ1OT1 participates in the regulation of cell proliferation and cell cycle, contributing to the cancer phenotype[20–24]. We found that silencing KCNQ1OT1 in HCT116 cells inhibited their growth. We then analyzed cell cycle distribution using flow cytometry to determine whether KCNQ1OT1 disrupts the cycle of HCT116 cells. Expectedly, the proportion of HCT116-siKCN cells in the G2/M phase decreased significantly. Thus, we confirmed that KCNQ1OT1 influences colon cancer progression.

lncRNAs, which lack protein-coding capacity, regulate mRNA processing both inside and outside the nucleus[25,26]. lncRNA can serve as a competing endogenous RNA (ceRNA) that interacts with RNA, DNA, and protein[13]. Therefore, we evaluated the molecular mechanisms through which KCNQ1OT1 affects the viability of HCT116 cells using RNA-Seq. To overcome the effects of a serum-based culture medium on cell proliferation, FBS was introduced into the medium at a low concentration 2 h before RNA isolation. We identified 577 DEGs, and DNA replication and mitotic cell cycle phase-related GO terms were enriched. KEGG pathway analysis results revealed that downregulated DNA replication- and cell cycle-associated DEGs were enriched in HCT116-siKCN cells. Furthermore, disease enrichment demonstrated that 102 DEGs were associated with colon carcinoma.

After screening downregulated DNA replication- and cell cycle-associated DEGs, we validated 19 genes using RT-qPCR assay. The results of this assay revealed that the expression of *PCNA*, *SKP2*, *ORC6*, *TTK*, *MCM3*, *MCM4*, *MCM7*, and *CCNE2* were decreased in HCT116-siKCN cells. Moreover, western blotting results confirmed that the expression of CCNE2 and PCNA was significantly downregulated in HCT116-siKCN cells. The roles of BCL2 family members in B-cell lymphoma-associated apoptosis were discovered in the 1980s[27]. BCL2 exerts anti-apoptotic effects that promote cancer development and progression. The BCL2 inhibitor, venetoclax, induces apoptosis and can be potentially used for treating various cancers, such as chronic lymphocytic leukemia[28]. Targeting BCL2 directly is designated as a valid chemotherapeutic strategy; however, understanding its molecular pathway of action would enable us to modify, manipulate, or mimic clinical treatments[29]. In the present study, reduced BCL2 expression was also observed in HCT116-siKCN cells. CASP3 is activated, while BCL2 expression is attenuated in tumor cell death[30]. Caspase-dependent intrinsic apoptosis inhibits BCL2 expression, and the reactivation of pro-apoptotic Bax and Bak proteins irreversibly triggers apoptosis[31,32]. To further explore whether caspase-dependent intrinsic apoptosis occurs in HCT116-siKCN cells, the expression of CASP3 was detected using western blotting. Interestingly, the expression of cleaved CASP3 was also reduced in HCT116-siKCN cells. We reviewed the RNA-Seq data but failed to analyze apoptosis-related DEGs. Thus, the role of CASP3 in KCNQ1OT1 regulation in HCT116 cells requires further determination.

Shen *et al.* reported that lncRNA KCNQ1OT1 targeted miR-34/Atg4B to induce KCNQ1OT1-mediated protective autophagy and chemoresistance in osteosarcoma[11]. BCL2 also plays an anti-autophagy role in cancer cells. Further research should explore the effects of autophagy on HCT116-siKCN cells. High KCNQ1OT1 expression is associated with poor overall survival of colon cancer patients. Wang *et al*. found that X-box binding protein 1, an important transcription factor that accelerates tumor growth, may

downregulate lncRNA KCNQ1OT1 expression in HCT116 cells [33]. Therefore, it is necessary to construct the upstream genes of lncRNA KCNQ1OT1 to investigate the targeted treatment of colon cancer.

The retroviral vector, pSEB61, was constructed by Prof. Tong-Chuan HE (University of Chicago), and the effectiveness was verified previously[34]. In the present study, we designed three retroviral vectors for pSEB61-siKCNQ1OT1 and packaged them into 293PA cells to silence lncRNA KCNQ1OT1 in HCT116 cells. HCT116-FLuc and HCT116-siKCN-FLuc cells were obtained after transfection with Ad-Fluc. Bioluminescence images *in vivo* showed similarities in the vitality of cells implanted in BALB/c nude mice. We found that the size of tumor xenografts was significantly decreased after the injection of HCT116-siKCN cells. Interestingly, tumor xenografts appeared almost non-existent at day 30 after implantation. These data suggest that silencing KCNQ1OT1 using the retroviral vector, pSEB61, may serve as a promising option for colon cancer therapy.Our study comprehensively analyzed the DEGs through bioinformatics and found scarcely oncogenicity through tumour xenograft silencing KCNQ1OT1 in HCT116 cells. However, the therapeutic effects of using vectors with silencing KCNQ1OT1 in the colon cancer model need to further study.

In conclusion, our study indicated that silencing KCNQ1OT1 in HCT116 cells may suppress colon cancer progression through the negative regulation of DNA replication and mitotic cell cycle phase-related pathways, targeting the downstream PCNA, CCNE2, and BCL2. KCNQ1OT1 may be a promising target for the treatment of colon cancer.

Methods

Cell lines and cell culture

The HCT116 cell line was procured from Procell (Wu Han, China) and cultured in complete McCoy's 5A medium (PM150710B, Procell). 293 Phoenix Ampho (293PA) and HEK-293 cells were kindly provided by Prof. Tong-Chuan HE (University of Chicago, Chicago, USA) and maintained in complete Dulbecco's Modified Eagle's medium-supplemented with 10% fetal bovine serum (FBS, Hyclone, CA, USA), 100 units of penicillin, and 100 mg of streptomycin-in an incubator at 37 °C with 5% CO_2.

Retrovirus production and stable cell lines

lncRNA-KCNQ1OT1 siRNA (siKCNQ1OT1) was designed and cloned into the pSEB61 vector (pSEB61-siKCNQ1OT1) and synthesized by Decoding Therapeutics Corp (Mt Prospect, USA). Retroviral vector pSEB61-siKCNQ1OT1 was packaged into a retrovirus in 293PA cells. Briefly, 293PA cells (70-80% density) were seeded onto 100-mm dishes. pSEB61-siKCNQ1OT1 and pCL-Ampho vectors were co-transfected into 293PA cells to harvest the retrovirus at intervals of 12 h. HCT116 cells, at a density of 50%, were infected with packaged retrovirus pSEB61-siKCNQ1OT1 concentrated using PEG8000 (89510, Sigma). Blasticidin S (0.5 μg/ml) selection yielded stable knockdown expression of KCNQ1OT1 or control cell lines, designated as HCT116-siKCN and HCT116-NC, respectively.

Total RNA extraction and real-time polymerase chain reaction (qPCR)

Total RNA was extracted using TRIzol Reagents (Invitrogen, Carlsbad, CA, USA) according to the manufacturer's instructions and used to generate cDNA templates via reverse transcription. qRT-PCR was performed as described in a instructions. The primers used in this study are shown in Table 1. SYBR Green-based qPCR analysis was carried out using the thermo cycler CXF-Connect (Bio-Rad, CA). *GAPDH* was used as an internal control.

RNA isolation, cDNA library construction, sequencing, and data analysis

Total RNA was extracted from HCT116 and HCT116-SiKCN cells using TRIzol reagent (Invitrogen) according to the manufacturer's instructions. After RNA quality was assessed using NanoDrop2000, mRNA was purified from total RNA using poly-T oligo-attached magnetic beads. The fragments per kilobase of transcript per million fragments mapped (FPKM) value was used to evaluate gene expression. Differentially expressed genes (DEGs) were identified using the tool Cuffdiff. The significant genes were selected based on the criteria of $|\log2(\text{fold change})| \geq 1$ and false discovery rate < 0.01. The statistical enrichment of DEGs in Gene Ontology (GO) and Kyoto Encyclopedia of Genes and Genomes (KEGG) pathways was compared to the whole genome background.

Immunofluorescence and Immunohistochemical staining

Immunofluorescence staining was performed as previously described instructions. Briefly, cells were fixed with paraformaldehyde, permeabilized with 0.1% Triton X-100, and blocked with 10% Block Aid^{TM} (B10710, Invitrogen), followed by incubation with primary antibodies against the following antigens: B-cell lymphoma 2 (BCL2) (1:200, ab182858, Abcam, CA, USA), proliferating cell nuclear antigen (PCNA) (1:200, ab92552, Abcam, CA, USA), and cyclin E2 (CCNE2) (1:200, ab40890, Abcam, CA, USA). Cells were then washed and incubated with 2 μg/mL Donkey Anti-Rabbit IgG (H+L) Highly Cross-Adsorbed Secondary Antibody, Alexa Fluor 594 (A-21207-1, Thermo Scientific,CA, USA) for immunofluorescence staining or ?????for immunohistochemical staining . Nuclei were counterstained with diamidino-2-phenylindole (DAPI) at a concentration of 1.43 μM. The stained cells were imaged using a laser scanning confocal microscope. Negative controls were stained without primary antibodies or with control IgG.

Western blotting

Total proteins were extracted and quantified using RIPA lysis buffer and a BCA detection kit (Beyotime, China) according to the manufacturer’s instructions. Next, equal amounts of protein were separated using 10% SDS-PAGE and transferred onto PVDF membranes (Millipore, Billerica, MA, USA). Subsequently, the membranes were blocked and incubated with primary antibodies against BCL2 (1:1000, ab182858, Abcam), caspase3 (CASP3) (1:1000, 9662s, Cell Signaling Technology), PCNA (1:1000, ab92552, Abcam), CCNE2 (1:1000, ab40890, Abcam), and GAPDH (1:1000, 8457s, Cell Signaling Technology) at 4 °C overnight and then with the appropriate peroxidase–conjugated secondary antibody at room

temperature . Chemiluminescence (Beyotime) reagent was used to detect the bands, and Image J software was employed for protein band quantification.

Crystal violet staining to determine cell proliferation

HCT116 and HCT116-siKCN cells were plated into 35-mm dishes at a density of 2 × 10^5 cells/dish and stained with crystal violet/formalin solution at 24, 48, 72, and 96 h for 20-30 min after gently washing with phosphate-buffered saline (PBS). Crystal violet was desorbed from the stained cells using acetic acid, following which the number of cells was quantified at 570-590 nm using a microplate reader.

Cell cycle distribution assay

HCT116 and HCT116-siKCN cells were digested with 0.25% trypsin and washed with 0.1 M PBS. Approximately 1 × 10^6 cells were fixed using 75% ethyl alcohol at 4 °C overnight. Cells were washed with cold PBS and then stained with propidium iodide (C1052, Beyotime) at 37 °C for 30 min in the dark. Cell analysis was performed using a flow cytometer (FACScan) equipped with CellQuest software (both from BD Biosciences).

In vivo bioluminescence tumor xenograft

All animal studies were conducted in accordance with the guidelines approved by the Ethics Committee of Wannan Medical College(No.2021012). Ad-FLuc was kindly provided by Prof. Tong-Chuan HE (University of Chicago). Both HCT116 and HCT116-siKCN cells were infected with Ad-Fluc to yield HCT116-FLuc and HCT116-siKCN-FLuc, respectively. Cells (1.5 × 10^7 per injection) were collected and injected subcutaneously into the flanks of 4–6-week-old BALB/c nude mice. After 2 and 14 days of injection, the animals were intraperitoneally injected with luciferase (ab145164, Abcam) and bioluminescence images were obtained using the Berthold LB983 imaging system. Data from bioluminescence images were analyzed using INDIGO software. Mice were sacrificed 20 days after injection, and the tumors were collected, making paraffin section for further analyses. Immunostaining with anti-PCNA (1:400, ab92552, Abcam) and anti-CCNE2 (1:400, ab40890, Abcam) was performed to detect the positive cells, which were quantified in three different high-power fields of each section.

Statistical analysis

All data are expressed as the mean ± standard deviation. The statistical analysis was performed using SPSS 22.0 software. The statistical significance of the data was evaluated using Student's *t*-test or one-way analysis of variance. $P < 0.05$ was considered statistically significant.

Declarations

ACKNOWLEDGEMENTS

The authors would like to thank Liwen He for carrying out ainimal studies in Chongqing Key Laboratory of Oral Diseases and Biomedical Sciences.

AUTHOR CONTRIBUTIONS

LS and TZ designed the experiment. GL contributed to the writing of the manuscript. LS and BW performed the experiments. ZW, and HZ analyzed the data. All authors read and approved the final manuscript.

COMPETING INTERESTS

The authors declare no competing interests.

DATA AVAILABILITY

All data generated or analyzed during this study are included in this published article

FUNDING

This work was financially supported by the Scientific research project of Anhui Provincial Health Commission in 2021 (# AHWJ2021b109 to LS), Scientific and Technological Research Program of Chongqing Municipal Education Commission (# KJZD-K201900402 to TZ) and Special Fund for Wannan Medical College Scholar Project (# WK2021F07)

CONSENT FOR PUBLICATION

All the authors listed have approved the manuscript that is enclosed.

ETHICS APPROVAL AND CONSENT TO PARTICIPATE

All animal studies were conducted in accordance with the guidelines approved by the Ethics Committee of Wannan Medical College.

References

1. Liu Y, Sharma S, Watabe K. Roles of lncRNA in breast cancer. Front Biosci (Schol Ed). 2015 Jun 1;7:94–108. doi: 10.2741/S427.
2. Ferreira HJ, Esteller M. Non-coding RNAs, epigenetics, and cancer: tying it all together. Cancer Metastasis Rev. 2018 Mar;37(1):55–73. doi: 10.1007/s10555-017-9715-8.
3. Yousefi H, Maheronnaghsh M, Molaei F, Mashouri L, Reza Aref A, Momeny M, Alahari SK. Long noncoding RNAs and exosomal lncRNAs: classification, and mechanisms in breast cancer metastasis and drug resistance. Oncogene. 2020 Jan;39(5):953–974. doi: 10.1038/s41388-019-1040-y.

4. Gil N, Ulitsky I. Regulation of gene expression by cis-acting long non-coding RNAs. Nat Rev Genet. 2020 Feb;21(2):102–117. doi: 10.1038/s41576-019-0184-5. Epub 2019 Nov 15.
5. Yao RW, Wang Y, Chen LL. Cellular functions of long noncoding RNAs. Nat Cell Biol. 2019 May;21(5):542–551. doi: 10.1038/s41556-019-0311-8.
6. Kopp F, Mendell JT. Functional Classification and Experimental Dissection of Long Noncoding RNAs. Cell. 2018 Jan 25;172(3):393–407. doi: 10.1016/j.cell.2018.01.011.
7. Hanly DJ, Esteller M, Berdasco M. Interplay between long non-coding RNAs and epigenetic machinery: emerging targets in cancer? Philos Trans R Soc Lond B Biol Sci. 2018 Jun 5;373(1748):20170074. doi: 10.1098/rstb.2017.0074.
8. Carlevaro-Fita J, Lanzós A, Feuerbach L, Hong C, Mas-Ponte D, Pedersen JS; PCAWG Drivers and Functional Interpretation Group, Johnson R; PCAWG Consortium. Cancer LncRNA Census reveals evidence for deep functional conservation of long noncoding RNAs in tumorigenesis. Commun Biol. 2020 Feb 5;3(1):56. doi: 10.1038/s42003-019-0741-7.
9. Huang H, Weng H, Chen J. m6A Modification in Coding and Non-coding RNAs: Roles and Therapeutic Implications in Cancer. Cancer Cell. 2020 Mar 16;37(3):270–288. doi: 10.1016/j.ccell.2020.02.004.
10. Wilson C, Kanhere A. The Missing Link Between Cancer-Associated Variants and LncRNAs. Trends Genet. 2021 May;37(5):410–413. doi: 10.1016/j.tig.2021.01.010.
11. Li Y, Li C, Li D, Yang L, Jin J, Zhang B. lncRNA KCNQ1OT1 enhances the chemoresistance of oxaliplatin in colon cancer by targeting the miR-34a/ATG4B pathway. Onco Targets Ther. 2019 Apr 9;12:2649–2660. doi: 10.2147/OTT.S188054.
12. Kang Y, Jia Y, Wang Q, Zhao Q, Song M, Ni R, Wang J. Long Noncoding RNA KCNQ1OT1 Promotes the Progression of Non-Small Cell Lung Cancer via Regulating miR-204-5p/ATG3 Axis. Onco Targets Ther. 2019 Dec 10;12:10787–10797. doi: 10.2147/OTT.S226044.
13. Chen S, Shen X. Long noncoding RNAs: functions and mechanisms in colon cancer. Mol Cancer. 2020 Nov 28;19(1):167. doi: 10.1186/s12943-020-01287-2.
14. Lee H, Zhang Z, Krause HM. Long Noncoding RNAs and Repetitive Elements: Junk or Intimate Evolutionary Partners? Trends Genet. 2019 Dec;35(12):892–902. doi: 10.1016/j.tig.2019.09.006.
15. Zhang X, Meyerson M. Illuminating the noncoding genome in cancer. Nat Cancer. 2020 Sep;1(9):864–872. doi: 10.1038/s43018-020-00114-3.
16. Goodall GJ, Wickramasinghe VO. RNA in cancer. Nat Rev Cancer. 2021 Jan;21(1):22–36. doi: 10.1038/s41568-020-00306-0.
17. Forrest ME, Saiakhova A, Beard L, Buchner DA, Scacheri PC, LaFramboise T, Markowitz S, Khalil AM. Colon Cancer-Upregulated Long Non-Coding RNA lincDUSP Regulates Cell Cycle Genes and Potentiates Resistance to Apoptosis. Sci Rep. 2018 May 9;8(1):7324. doi: 10.1038/s41598-018-25530-5.
18. Pauler FM, Koerner MV, Barlow DP. Silencing by imprinted noncoding RNAs: is transcription the answer? Trends Genet. 2007 Jun;23(6):284–92. doi: 10.1016/j.tig.2007.03.018.

19. Kornienko AE, Guenzl PM, Barlow DP, Pauler FM. Gene regulation by the act of long non-coding RNA transcription. BMC Biol. 2013 May 30;11:59. doi: 10.1186/1741-7007-11-59.
20. Lin ZB, Long P, Zhao Z, Zhang YR, Chu XD, Zhao XX, Ding H, Huan SW, Pan YL, Pan JH. Long Noncoding RNA KCNQ1OT1 is a Prognostic Biomarker and mediates CD8 + T cell exhaustion by regulating CD155 Expression in Colorectal Cancer. Int J Biol Sci. 2021 Apr 22;17(7):1757–1768. doi: 10.7150/ijbs.59001.
21. Cagle P, Qi Q, Niture S, Kumar D. KCNQ1OT1: An Oncogenic Long Noncoding RNA. Biomolecules. 2021 Oct 29;11(11):1602. doi: 10.3390/biom11111602.
22. Zhang S, Ma H, Zhang D, Xie S, Wang W, Li Q, Lin Z, Wang Y. LncRNA KCNQ1OT1 regulates proliferation and cisplatin resistance in tongue cancer via miR-211-5p mediated Ezrin/Fak/Src signaling. Cell Death Dis. 2018 Jul 3;9(7):742. doi: 10.1038/s41419-018-0793-5.
23. Yang F, Qin Y, Lv J, Wang Y, Che H, Chen X, Jiang Y, Li A, Sun X, Yue E, et al. Silencing long non-coding RNA Kcnq1ot1 alleviates pyroptosis and fibrosis in diabetic cardiomyopathy. Cell Death Dis. 2018 Sep 24;9(10):1000. doi: 10.1038/s41419-018-1029-4.
24. Shen Y, Xu J, Pan X, Zhang Y, Weng Y, Zhou D, He S. LncRNA KCNQ1OT1 sponges miR-34c-5p to promote osteosarcoma growth via ALDOA enhanced aerobic glycolysis. Cell Death Dis. 2020 Apr 24;11(4):278. doi: 10.1038/s41419-020-2485-1.
25. Palazzo AF, Koonin EV. Functional Long Non-coding RNAs Evolve from Junk Transcripts. Cell. 2020 Nov 25;183(5):1151–1161. doi: 10.1016/j.cell.2020.09.047.
26. Nair L, Chung H, Basu U. Regulation of long non-coding RNAs and genome dynamics by the RNA surveillance machinery. Nat Rev Mol Cell Biol. 2020 Mar;21(3):123–136. doi: 10.1038/s41580-019-0209-0.
27. Warren CFA, Wong-Brown MW, Bowden NA. BCL-2 family isoforms in apoptosis and cancer. Cell Death Dis. 2019 Feb 21;10(3):177. doi: 10.1038/s41419-019-1407-6.
28. Bednarz-Misa I, Diakowska D, Szczuka I, Fortuna P, Kubiak A, Rosińczuk J, Krzystek-Korpacka M. Interleukins 4 and 13 and Their Receptors Are Differently Expressed in Gastrointestinal Tract Cancers, Depending on the Anatomical Site and Disease Advancement, and Improve Colon Cancer Cell Viability and Motility. Cancers (Basel). 2020 Jun 4;12(6):1463. doi: 10.3390/cancers12061463.
29. Tambaro FP, Wierda WG. Tumour lysis syndrome in patients with chronic lymphocytic leukaemia treated with BCL-2 inhibitors: risk factors, prophylaxis, and treatment recommendations. Lancet Haematol. 2020 Feb;7(2):e168-e176. doi: 10.1016/S2352-3026(19)30253-4.
30. Van Opdenbosch N, Lamkanfı M. Caspases in Cell Death, Inflammation, and Disease. Immunity. 2019 Jun 18;50(6):1352–1364. doi: 10.1016/j.immuni.2019.05.020.
31. Vince JE, De Nardo D, Gao W, Vince AJ, Hall C, McArthur K, Simpson D, Vijayaraj S, Lindqvist LM, Bouillet P, et al. The Mitochondrial Apoptotic Effectors BAX/BAK Activate Caspase-3 and – 7 to Trigger NLRP3 Inflammasome and Caspase-8 Driven IL-1β Activation. Cell Rep. 2018 Nov 27;25(9):2339–2353.e4. doi: 10.1016/j.celrep.2018.10.103.

32. Zhang Z, Zhang Y, Xia S, Kong Q, Li S, Liu X, Junqueira C, Meza-Sosa KF, Mok TMY, Ansara J, et al. Gasdermin E suppresses tumour growth by activating anti-tumour immunity. Nature. 2020 Mar;579(7799):415–420. doi: 10.1038/s41586-020-2071-9.
33. Wang Y, Zhang J, Zheng S. The role of XBP-1-mediated unfolded protein response in colorectal cancer progression-a regulatory mechanism associated with lncRNA-miRNA-mRNA network. Cancer Cell Int. 2021 Sep 14;21(1):488. doi: 10.1186/s12935-021-02167-5.
34. Deng F, Chen X, Liao Z, Yan Z, Wang Z, Deng Y, Zhang Q, Zhang Z, Ye J, Qiao M, et al. A simplified and versatile system for the simultaneous expression of multiple siRNAs in mammalian cells using Gibson DNA Assembly. PLoS One. 2014 Nov 14;9(11):e113064. doi: 10.1371/journal.pone.0113064.

Tables

Table 1. List of primers used for qPCR analysis

Gene symbol	Gene name	Primer (5’-3’)
SKP2 Homo	S-phase kinase associated protein 2	F: TGCTAAGCAGCTGTTCCAGA R: AAGATTCAGCTGGGTGATGG
CCNE2 Homo	cyclin E2	F: GGGGATCAGTCCTTGCATTA R:CCCAGCTTAAATCAGGCAAA
PCNA Homo	proliferating cell nuclear antigen	F: GGCGTGAACCTCACCAGTAT R: TTCTCCTGGTTTGGTGCTTC
ORC6 Homo	origin recognition complex subunit 6	F: GCAGTGAACATGGCTTCAAA R: AGCAGTGCAGCAGAAGTGAA
TTK Homo	TTK protein kinase	F: CAGCAGCAACAGCATCAAAT R: TGCTTGAACCTCCACTTCCT
MCM3 Homo	minichromosome maintenance complex component 3	F: AGCTTCTGCGGTATGTGCTT R: CCTGTTTCCTGGTCTGTGGT
MCM4 Homo	minichromosome maintenance complex component 4	F: TTGAAGCCATTGATGTGGAA R: GGCACTCATCCCCGTAGTAA
MCM7 Homo	minichromosome maintenance complex component 7	F: CGGTGCTGGTAGAAGGAGAG R: AAACCCTGTACCACCTGTCG
GAPDH Homo	glyceraldehyde-3-phosphate dehydrogenase	F: CAGCGACACCCACTCCTC R: TGAGGTCCACCACCCTGT

Figures

Figure 1

HCT116-siKCN stable cell line with the retroviral vector pSEB61.

(A) Sequence alignment of three lncRNA KCNQ1OT1 siRNAs. (B) Plasmid map showing the introduction of the retroviral vector pSEB61 into the established HCT116-siKCNQ1OT1 cell line. (C) Morphology of HCT116-NC and HCT116-siKCN cells. Bar = 150 μm. (D) Confirmation of KCNQ1OT1 silencing in HCT116 cells using RT-qPCR. *GAPDH* was used as an internal control (*t*-test, $^{**}P < 0.01$).

Figure 2

Effects of KCNQ1OT1 silencing on cell proliferation and cell cycle in HCT116 cells. (A) Cell proliferation was assessed using crystal violet staining assay. HCT116-NC and HCT116-siKCN cells were seeded onto 35-mm dishes at a low density. Attached cells were fixed with 4% paraformaldehyde for crystal violet staining at 24, 48, 72, and 96 h. (B) Crystal violet was desorbed from the stained cells using 10% acetic acid, following which the number of cells was quantified at A570–A590 nm in three independent assays. The HCT116-siKCN cell line displayed significantly fewer cells at 48, 72, and 96 h than the HCT116-NC cell line. (C) Cell cycle progression was assessed using flow cytometry (FCM), the results of which revealed cell cycle arrest at the S/G2/M phase in HCT116-siKCN cells. (D) The cell cycle profiles of representative FCM data are shown here. Data are presented as the mean ± SEM, compared with NC, $^{***}P < 0.001$.

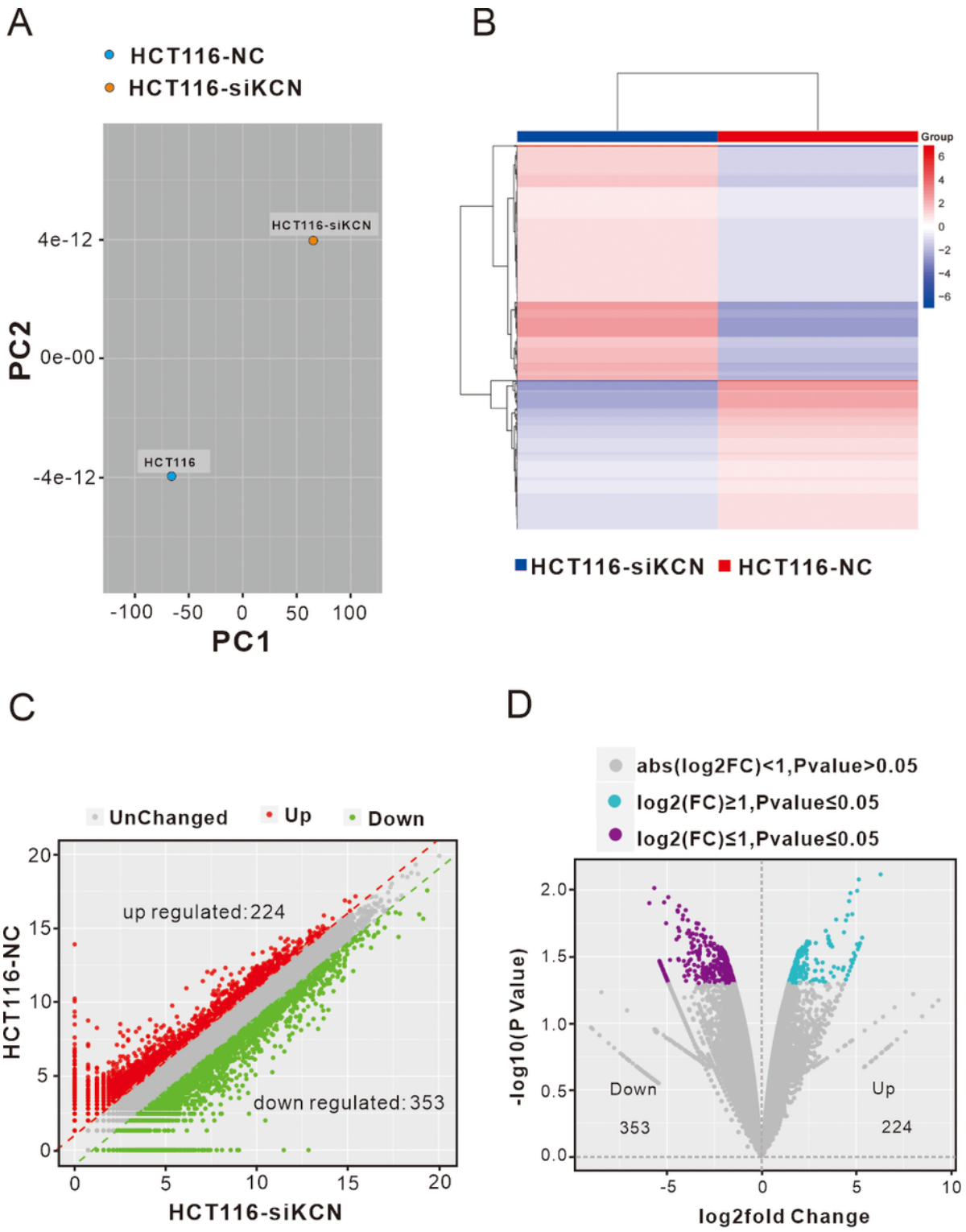

Figure 3

Analysis of differentially expressed genes (DEGs) between HCT116-NC and HCT116-siKCN cells. (A) The PCA diagram exhibited the similarity degree between samples through dimensional reduction. (B) The correlation between HCT116-NC and HCT116-siKCN cells was determined using Hierarchical cluster heatmap analysis of DEG expression. The color scale in the heat map represents the relative intensity of metabolite changes. Red indicates upregulated genes, while blue indicates downregulated genes. (C-D)

We found 244 upregulated (red dots) DEGs and 353 downregulated (green dots) DEGs in the two cell lines using Scatter (C) and Volcano plots (D).

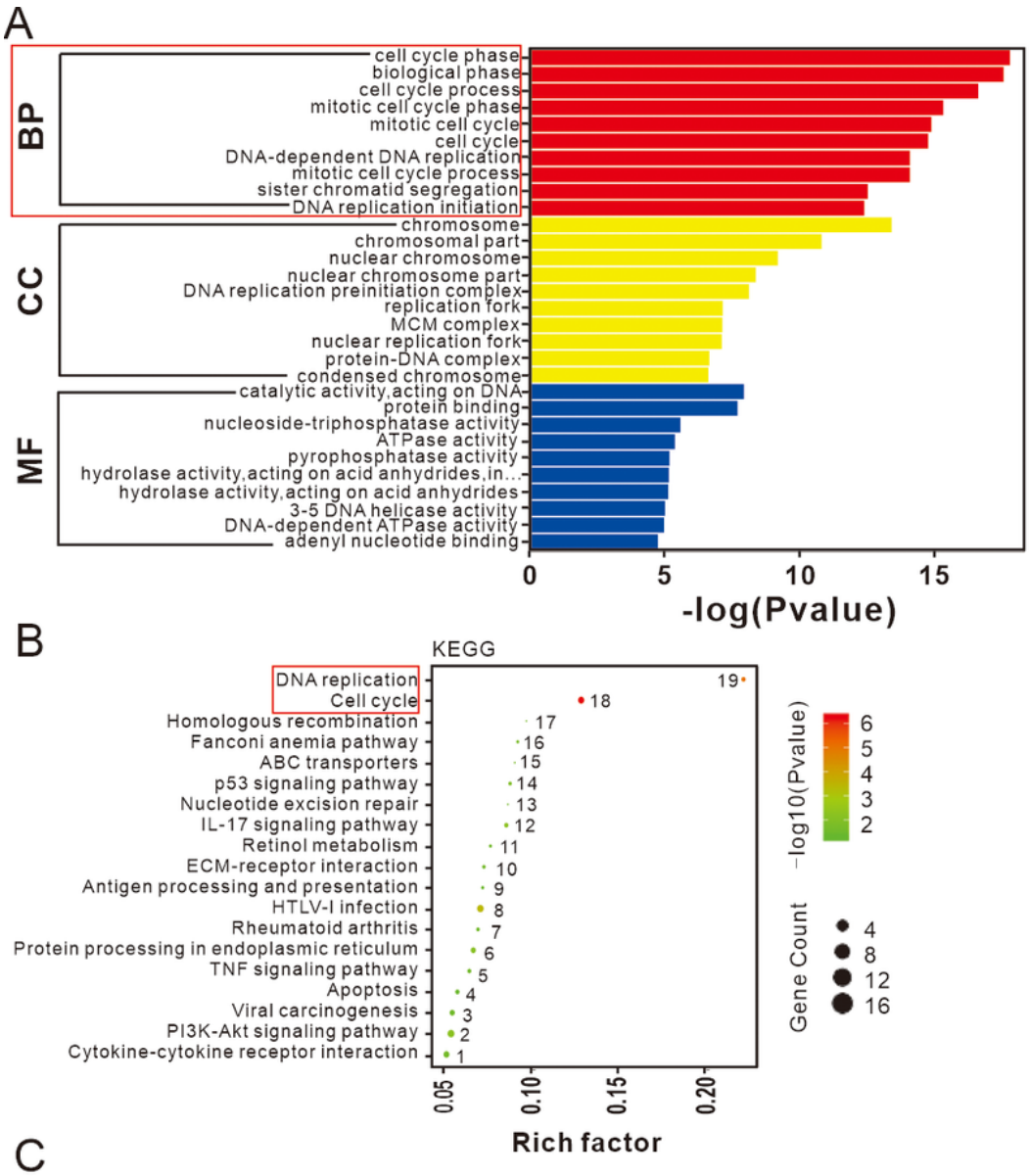

C

Disease_id	Disease_name	Annotated	Significant	rich_factor
C0006142	Malignant neoplasm of breast	4584	189	0.041230366
C0027627	Neoplasm Metastasis	3766	162	0.043016463
C0678222	Breast Carcinoma	4471	183	0.040930441
C0699790	Colon Carcinoma	1993	102	0.051179127
C0026764	Multiple Myeloma	1270	74	0.058267717
C1140680	Malignant neoplasm of ovary	2020	101	0.05
C2239176	Liver carcinoma	3365	144	0.042793462
C0029925	Ovarian Carcinoma	2051	100	0.048756704
C0005684	Malignant neoplasm of urinary bladder	1360	74	0.054411765
C0596263	Carcinogenesis	3929	158	0.040213795

Figure 4

Gene ontology (GO), Kyoto Encyclopedia of Genes and Genomes (KEGG), and disease enrichment analysis results of differentially expressed genes (DEGs) using RNA sequencing. (A) GO term enrichment

analysis of DEGs. The bar plot indicates enrichment scores of the top ten genes significantly enriched in biological processes, cellular components, and molecular functions. (B) Top 19 signaling pathways identified in KEGG enrichment pathway analysis of DEGs. (C) Top ten disease enrichment pathways of lncRNA-KCNQ1OT1. In total, 102 DEGs were identified in colon carcinoma.

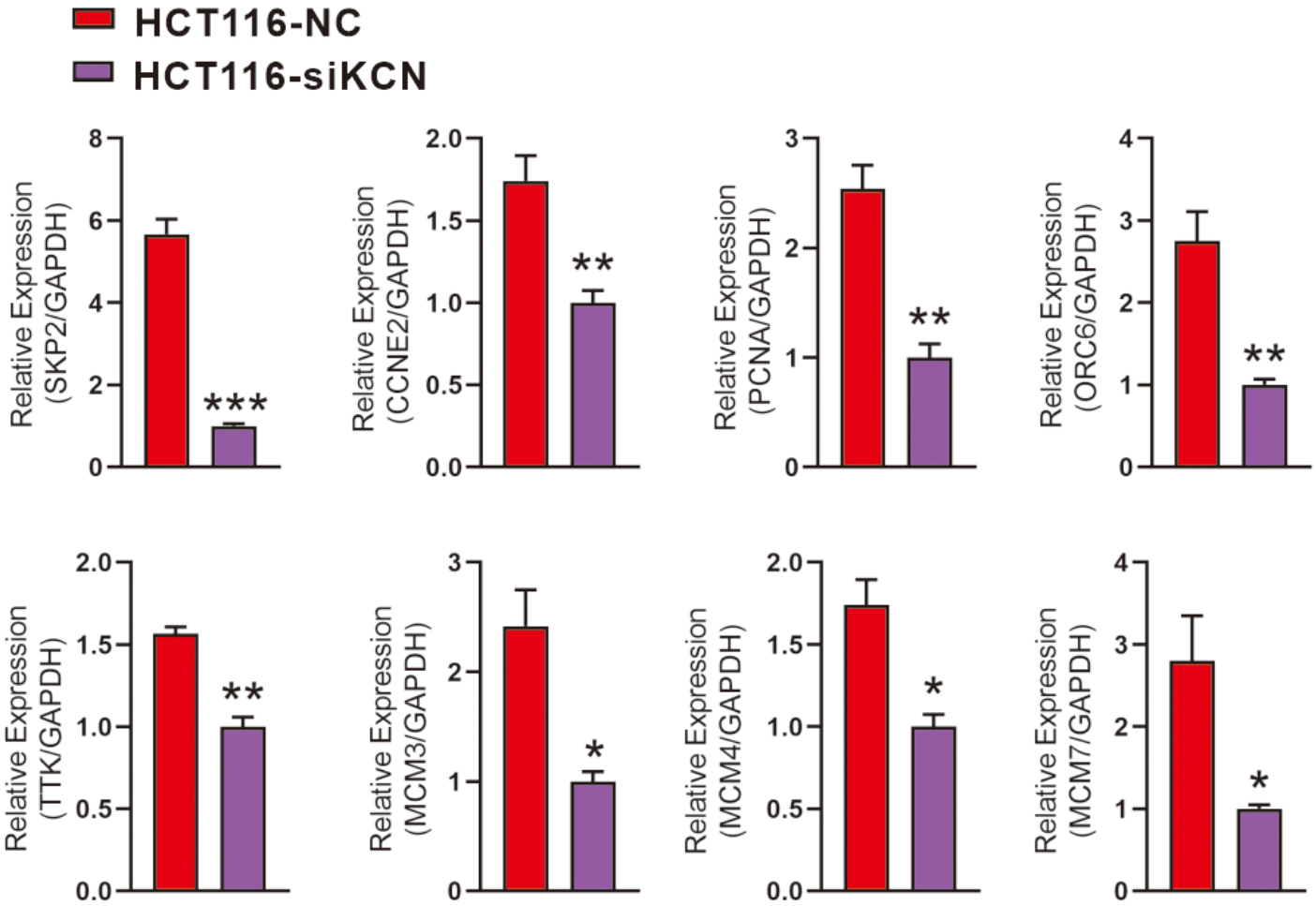

Figure 5

Validation of downstream genes involved in DNA replication and cell cycle pathways using RT-qPCR. RT-qPCR performed using primers for *SKP2*, *CCNE2*, *PCNA*, *ORC6*, *TTK*, *MCM3*, *MCM4*, *MCM7*, and *GAPDH*. Expression of *PCNA*, *SKP2*, *ORC6*, *TTK*, *MCM3*, *MCM4*, *MCM7*, and *CCNE2* decreased in HCT116-siKCN cells. Each assay was performed in triplicate and compared with the corresponding HCT116-NC cell control group, *$P < 0.05$, **$P < 0.01$, and ***$P < 0.001$

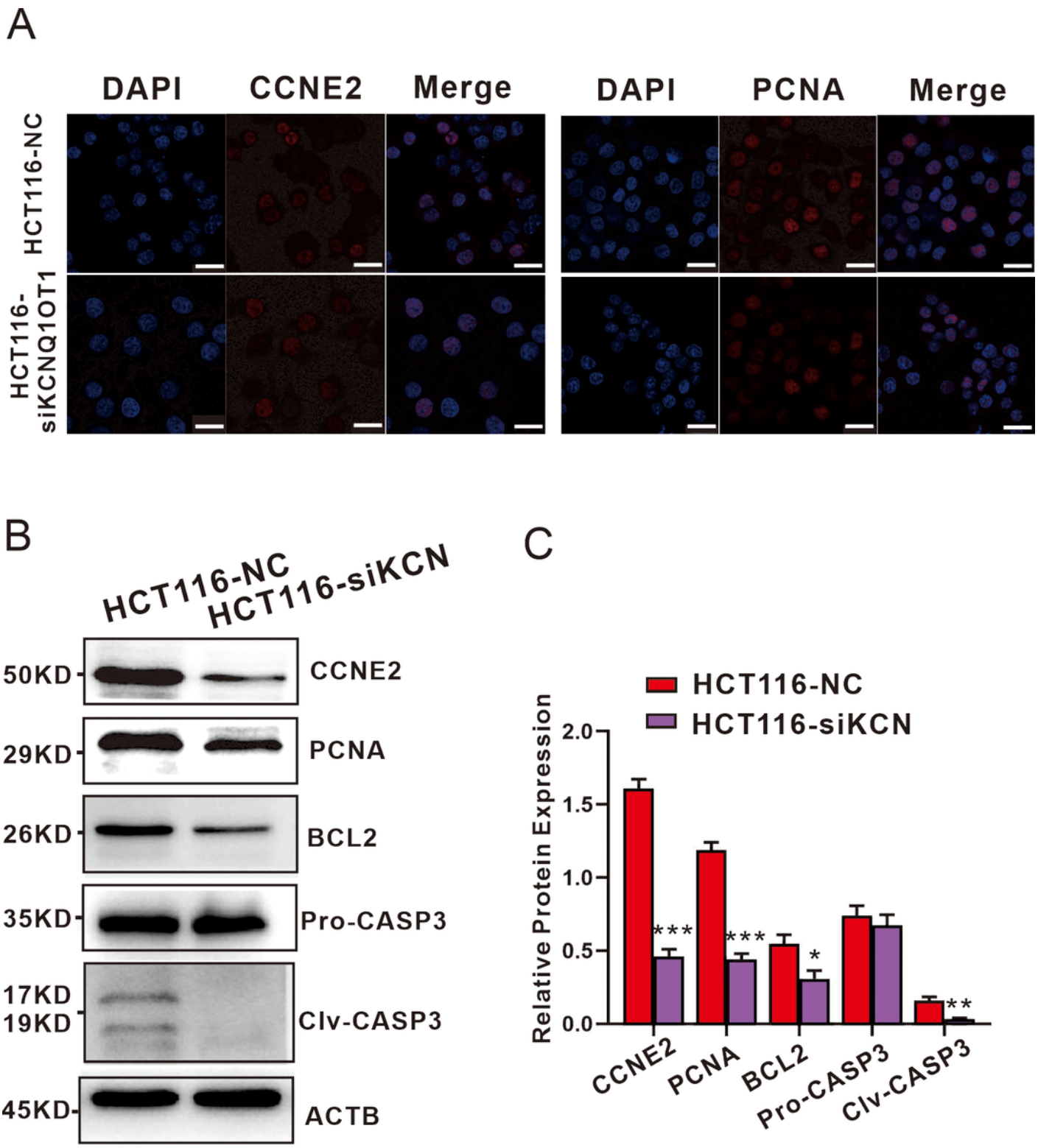

Figure 6

Validation of downstream targets involved in DNA replication and cell cycle pathways using immunofluorescent staining and western blotting. (A) Immunofluorescent staining (red) results indicated that CCNE2 and PCNA exhibited strongly positive expression in the nucleus. Nuclei were stained blue using DAPI. Bar = 25 μm. (B) Western blotting results showing CCNE2, PCNA, BCL-2, and CASP3 expression in two groups. β-Actin was used to confirm equal loading. (C) Representative quantitative

western blotting results are shown. Compared with HCT116-NC cells, CCNE2, PCNA, BCL-2, and cleaved CASP3 levels were decreased in HCT116-siKCN cells. (*t*-test, **P* < 0.05, ***P* < 0.01, ****P* < 0.001).

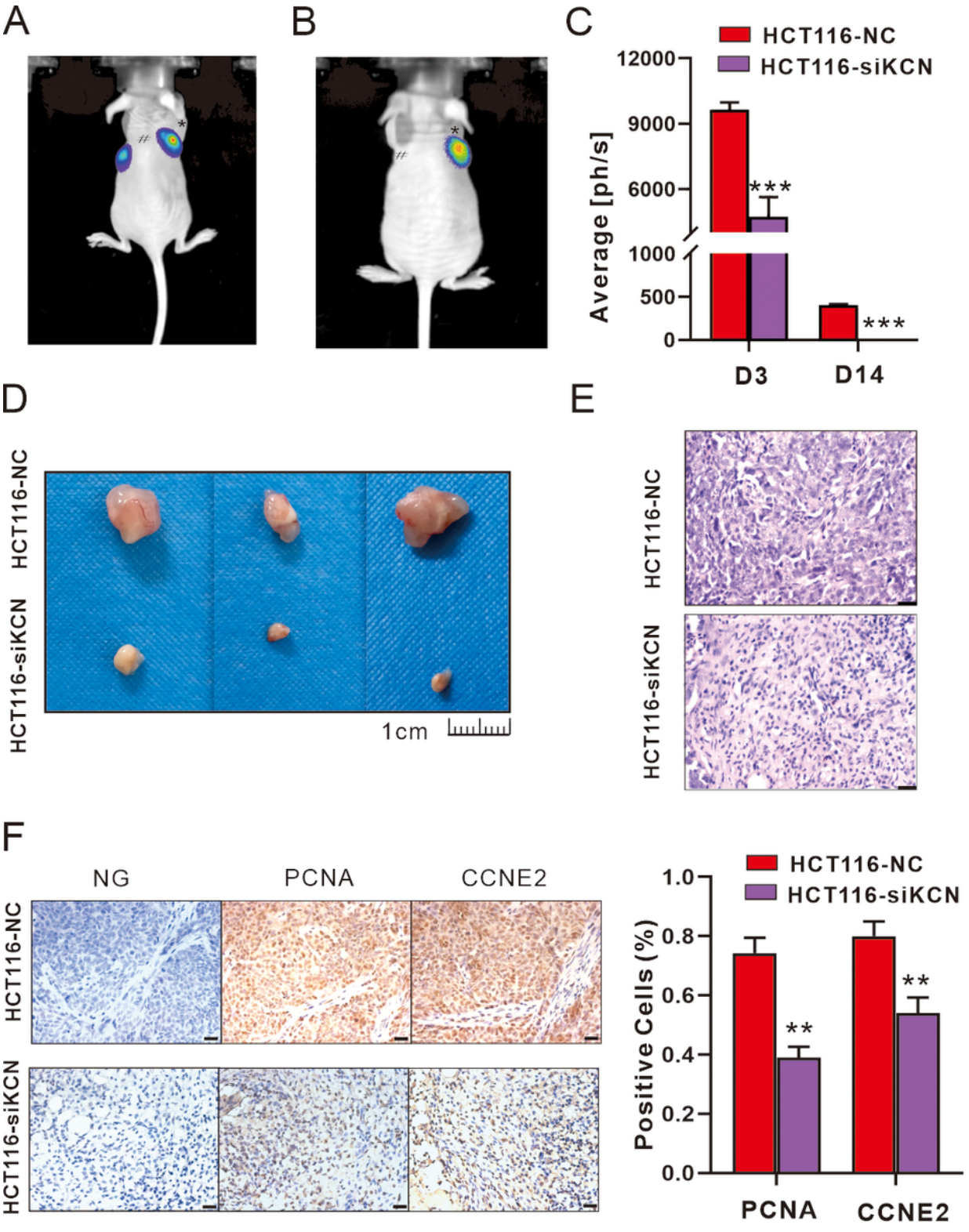

Figure 7

siRNA-KCNQ1OT1 ablates cell vitality and tumor xenograft *in vivo.* Tumor growth bioluminescence imaging was performed during the peak time point after the intraperitoneal injection of 140 mg/kg d-

fluorescein sodium salt on days 3 (A) and 14 (B) of cell inoculation. The imaging exposure time was 60 s. # represents HCT116 cells, while * represents HCT116-siKCN cells. (C) Images of subcutaneous tumors of HCT116-NC and HCT116-siKCN group mice on day 20 after injection.(D) Representative quantitative tumor average photon/s statistical analyses are shown. (*t*-test, ***$P < 0.001$). (E) Hematoxylin and eosin staining of sections from tumor xenograft. Bar=25 μm. (F) CCNE2 and PCNA staining and quantification of positive cell. Bar=25 μm. (*t*-test, ***$P < 0.001$)